Developing a novel binderless diamond grinding wheel with femtosecond laser ablation and evaluating its performance in grinding soft and brittle materials

Qu, M., Jin, T., Xie, G. & Cai, R.

Original citation & hyperlink:
Qu, M, Jin, T, Xie, G & Cai, R 2020, 'Developing a novel binderless diamond grinding wheel with femtosecond laser ablation and evaluating its performance in grinding soft and brittle materials' Journal of Materials Processing Technology, vol. 275, 116359.
https://dx.doi.org/10.1016/j.jmatprotec.2019.116359

DOI 10.1016/j.jmatprotec.2019.116359
ISSN 0924-0136

Publisher: Elsevier

Developing a novel binderless diamond grinding wheel with femtosecond laser ablation and evaluating its performance in grinding soft and brittle materials

Meina Qu[a, b], Tan Jin[a, b], Guizhi Xie[a,b,*], Rui Cai[c]

[a]National Engineering Research Centre for High Efficiency Grinding, Hunan University, Changsha, Hunan 410082, China

[b]College of Mechanical and Vehicle Engineering, Hunan University, Changsha, Hunan 410082, China

[c]School of Mechanical, Aerospace and Automotive Engineering Faculty of Engineering Environment and Computing, Coventry University, 3 Gulson Road, Coventry, CV1 2JH, UK

* Corresponding author. Tel.: +86 731 88821833. E-mail address: guizhixie@aliyun.com

Abstract: In this study, a binderless diamond grinding wheel (BDGW) is fabricated to prevent impurities embedding during the machining of soft and brittle materials by conventional grinding wheels. The 'binder' features, as well as the 'grains', are produced on a single piece of chemical vapor deposition diamond, whilst the 'grains' are ablated with a femtosecond laser. The performance of the novel grinding tool in terms of grinding radio, wear types, grinding forces and specific grinding energy, ground surface roughness, surface morphology, and subsurface damage is evaluated by comparing it with a resin-bonded diamond grinding wheel (RDGW). Experimental results show that the BDGW has excellent redress life with simple form of wear-abrasion wear on the top of the cutting edges and extremely high grinding radio of 10^3, which is nearly eight times of that of the RDGW. The benefit of the simple form of BDGW wear is that no embedded bond debris and fall-off grains appear. These conditions are essential to ensuring high ground surface quality for grinding soft and brittle materials.

Keyword: Chemical vapor deposition diamond; Femtosecond laser ablation; Binderless diamond grinding wheel; Grinding performance

1. Introduction

Photoelectric crystals, such as potassium dihydrogen phosphate (KDP), potassium titanium oxide phosphate, and lithium niobate crystals ($LiNbO_3$), are widely used in the semiconductor and laser industries due to their unique non-linear opto-electrical qualities. Bespalov et al. (1997) used a rapid-growth technology to grow KDP

crystal samples with sizes and quality that are close to the requirements of inertial confinement fusion laser drivers. Randles et al. (2008) presented a process technology to form thin diaphragms with sealed cavities in a $LiNbO_3$ wafer. Grinding is an effective method to machine these crystals with high process efficiency. Namba (1998) achieved smooth optical surface (RMS and PV values of 1.93 nm and 12.6 nm, respectively) on a KDP test piece with a SD5000-75-B diamond wheel. Chen et al. (2016) proposed a hybrid machining method by combining precision grinding with fly cutting to form the chamfered faces of KDP crystal, improving machining efficiency nearly five times. Qu et al. (2019) used a resin-bonded diamond grinding wheel with Ni-P alloy coating on the abrasive grains to remove the surface material of KDP components with high process efficiency and low damage. However, the use of conventional grinding wheels is often constrained by impurities, such as debris from bond materials and lose grains embedded into ground surfaces due to the low hardness of these photoelectric crystals.

Conventional diamond grinding wheels consists of bond, abrasive grains and pores. Diamond grains are bonded in the wheels with bonding materials, such as resin, vitrified or metal bonds. In grinding, bond debris and loose and broken grains often fall off to the ground surface and become embedded to it, which is of great concern to the final ground surface quality, especially in soft and brittle materials. Loose and broken grains are normally caused by dressing and high grinding forces during grinding, particularly when grains distribute randomly on grinding wheel surfaces with inconsistent protrusion heights. Subsequently, cutting loads on individual grains vary remarkably, and early grain breakage and pull-out from the wheel body subsequently occurs under

certain grinding conditions. Using engineered diamond grinding wheels with prearranged distribution patterns of grains to improve the uniformity of wheel surface topography, enhance process performance and prevent loose and broken grains from falling off have been proposed. Aurich et al. (2008) using a kinematic simulation method an electroplated diamond grinding wheel with a defined grain pattern for dry grinding condition, developed. Heinzel and Rickens (2009) investigated the properties of an electroplated diamond grinding wheel with defined grain placement for machining optical glass. The process of planting abrasive grains on these grinding wheels is extremely complicated. Tawakoli et al. (2007) used a single-point diamond to dress a resin-bonded CBN grinding wheel to produce microstructures on the wheel surface and thus reduce heat generation during dry grinding. Walter et al. (2014) proposed a novel laser structuring method utilizing a pulsed picosecond laser and used it to produce various micropatterns on a CBN grinding wheel. These studies showed that grains crack easily and broken grains are embedded in ground surfaces when used for grinding soft and brittle crystals.

Chemical vapor deposition (CVD) diamond is a good abrasive layer for making binderless grinding wheels owing to its large size, reasonable strength and toughness, hardness comparable to that of single crystal diamond (SCD) and lower cost as compared with that of SCD. Gäbler et al. (2000) presented new cemented carbide microtools with CVD diamond coatings for grinding brittle materials and drilling printed circuit boards. Gäbler and Pleger (2010) produced two peripheral CVD diamond-coated grinding wheels with 80 mm diameters through hot filament chemical

vapor deposition. Brinksmeier et al. (2012) manufactured CVD diamond-coated grinding wheels and successfully used in machining brittle and hard materials, such as optical glass (N-BAK2) and PCBN. These grinding wheels are easily blocked by grinding debris due to the polycrystalline diamond surface morphology. Guo et al. (2018) used laser ablation technology to construct groves with 4-6 μm width and 8 μm depth on the surface of CVD diamond-coated grinding wheel to solve the grinding wheel blockage issue. The CVD diamond coating easily falls off from the hub of these grinding wheels. Butler-Smith et al. (2012) innovatively designed and fabricated a micro-grinding tool on a CVD diamond by laser ablation; the tool had excellent redress life for grinding Ti-6Al-4V, but a graphite layer was produced on the surface of the micro-grinding tool due to laser thermal damage.

In this study, a novel diamond grinding wheel without a bonding system is fabricated on a CVD diamond with femtosecond laser. The 'binder' features and the 'grains' are produced on a single piece of CVD diamond, whilst the 'grains' are micro-processed using femtosecond laser. Compared with conventionally engineered grinding wheels, the proposed wheel has the following features: (1) bond, abrasives and pore in the wheel structure; (2) superhardness and excellent redress life; (3) high protrusion height and (4) adjustable shape, size, quantity and grain distribution.

The grinding radio G, wear types, grinding forces and specific grinding energy (SGE; F_n, F_t, F_n/F_t and e_s) of the binderless diamond grinding wheel (BDGW); ground surface morphology; ground surface roughness and subsurface damage are evaluated by comparing them with those of a resin-bonded diamond grinding wheel (RDGW)

under different grinding conditions.

2. Grinding wheel fabrication

2.1 Preparation of abrasive layers

In this study, a large size of CVD diamond, produced by Biejing Tandi Orient Superhard Materials co., LTD. is selected as the abrasive layer of the BDGW. In a CVD diamond, the growing surface is more suitable than the basal surface for grain growth. Harniman et al. (2015) investigated electron emission from a set of CVD diamond films with high-resolution peak force-controlled tunnelling atomic force microscopy. The growth surface is selected as the working surface for the grinding tool. Although numerous sharp grain protrusions are found on the original growth surface, the distribution of grains on this surface are uneven, and the protrusion height too small to meet the material removal requirements as a grinding tool (Fig. 1a).

To make grains with sharp cutting edges on the growth surface by using laser in the later process, thermal chemical polishing (TCP) is used in the polishing of the CVD diamond. The details of the TCP technique can be found in the study of Malshe et al. (1999). The roughness R_a of the CVD diamond is improved from 6.0 μm before polishing to 80 nm after polishing. After polishing, the growth surface is reasonably smooth and flat, but residual holes or cracks are still present because of imperfect grain combinations (Fig. 1b).

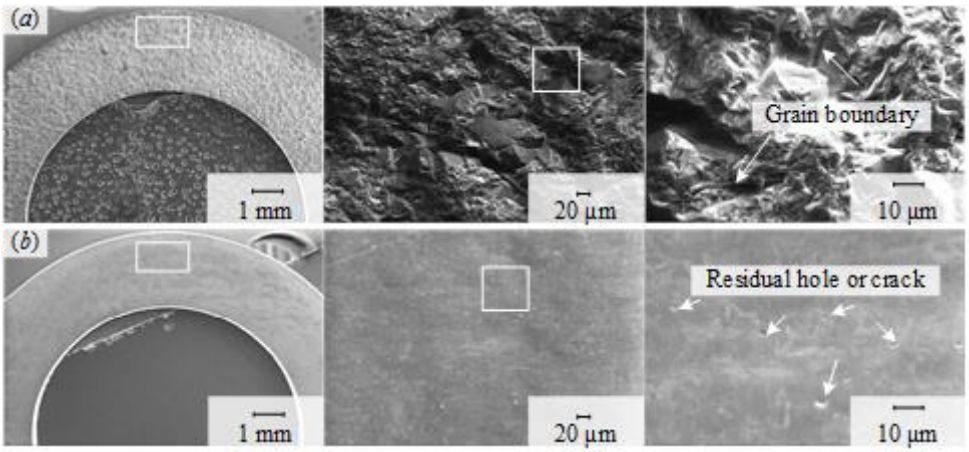

Fig. 1 Morphology of CVD diamond on the growth surface, (*a*) before polishing and (*b*) after polishing

2.2 Laser ablation

In this study, the CVD diamond abrasive layer is ablated with a Q-pulse ultraviolet and femtosecond laser. Laser ablation parameters, such as Q-pulse ultraviolet and femtosecond laser, are shown in Table 1. The machining platform of the Q-pulse ultraviolet is equipped with a vibration-mirror laser scanning system. The laser focus moves according to an arranged tool path to produce the required removal patterns on the working area (Fig.2a). Fig.2b shows the machining platform of the femtosecond laser. Compared with the Q-pulse ultraviolet laser, femtosecond laser has extremely short pulse and extremely high single-pulse energy and can generate high power density at relatively low laser power.

Table 1 Laser ablation parameters of Q-pulse ultraviolet and femtosecond lasers

Laser device	Q-pulse ultraviolet	Femtosecond laser
Trigger mode	Pulsed	Pulsed
Average power	7 W	11.1 W
Wavelength	355 nm	1030 nm

Pluse width	18 ns	250 fs
Repetition frequency	30 kHz	175 kHz
Diameter of laser spot	35 μm	30 μm
Scanning speed	0.8 m/s	2 m/s
Adjacent laser ablation track spacing	20 μm	12 μm

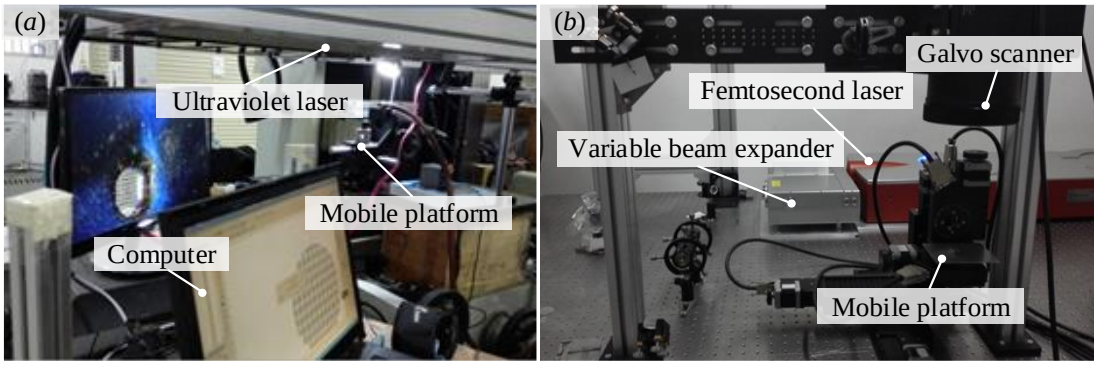

Fig. 2 Laser processing platform of (*a*) Q-pulse ultraviolet and (*b*) femtosecond lasers

Figs. 3a and 3b show the grains on the CVD diamond surface produced by Q-pulse ultraviolet laser with different machining parameters. The minimum width of the grains can be controlled at approximately 50 μm. A graphite layer is observed after laser ablation due to the thermal effects of laser machining. A silicon carbide grinding wheel with average abrasive grit size of 15 μm is applied to remove the graphite layer under the following machining parameters: grinding wheel speed v_s = 15 m/s, worktable speed v_w = 1 mm/s, grinding depth a_p = 2 μm and total cutting depth = 20 μm. After removing the graphite layer, the grains are seriously damaged and hardly noticeable due to their over-dense spacing (32 mm^{-2}; Fig. 3a). Due to low grain density (approximately 16 mm^{-2}), the grains became clear after graphite removal but with apparent grain fractures (Fig. 3b). Fig. 3c shows the grains produced by a femtosecond laser at grains density of 16 mm^{-2}. The grains in this case are controlled at a width of 10 μm with no thermal damage, that is, no graphite layer is produced.

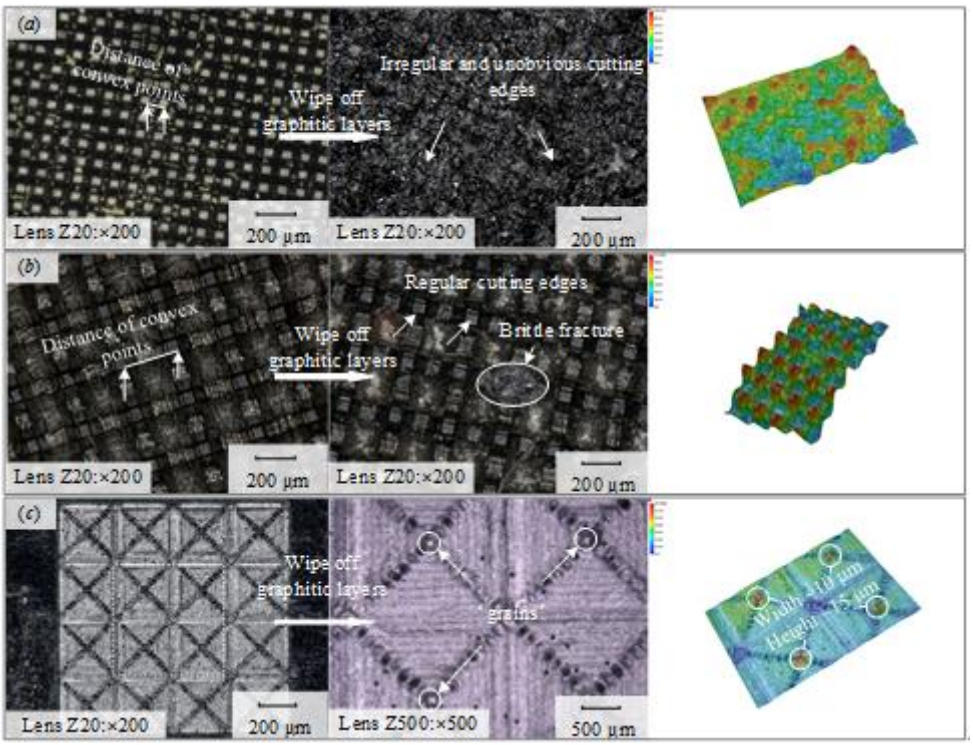

Fig. 3 Microstructure of CVD diamond surface by (*a*) Q-pulse ultraviolet laser at 32 grains per mm^2, (*b*) Q-pulse ultraviolet at 16 grains per mm^2 and (*c*) femtosecond laser at 16 grains per mm^2

2.3 Binderless diamond grinding wheel

The abrasive layer of the cup wheel is fabricated. The polished CVD diamond is cut into a ring with an inner diameter of 10 mm, outer diameter of 16 mm and thickness of 3 mm. A femtosecond laser is selected to produce grains on the abrasive layer. Fig. 4 shows the grains on the surface of the CVD ring produced by a femtosecond laser. On the surface of the abrasive layer, the grains are arranged in the periodic distributed rectangular areas, and the surrounding rectangular areas are designed to accommodate grinding chips. The grains are in a pyramid shaped similar to the ideal abrasive grains of a conventional grinding wheel. The average size of the grains is approximately 38 μm, which is in accordance with that of the conventional grinding wheel used to correct the optical axis of KDP crystal (Qu et al., 2019). The protrusion height of the grains are approximately 16 μm. After laser ablation, the CVD diamond abrasive layer is attached

with the tool holder by adhesive bonding. The round runout of the binderless grinding wheel is controlled within 10 μm.

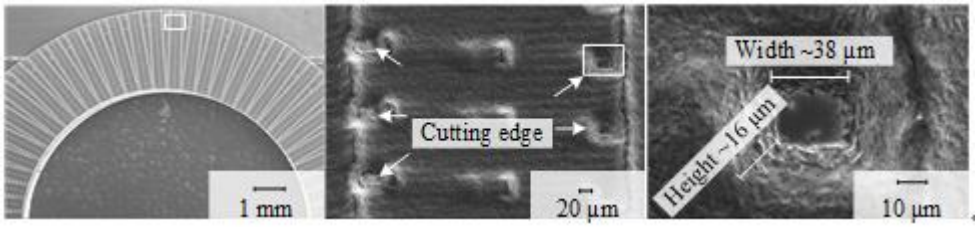

Fig. 4 Topography of the BDGW

3. Grinding performance experiment

3.1 Workpiece material

The workpiece material is the KDP crystal, a typical soft and brittle material, which is widely applied in Q-switches, high-speed photography shutters and frequency harmonic generation lens.

3.2 Grinding platform

Grinding experiments are performed on a precision *CNC* grinding machine (Fig. 5*a*). The machine has six CNC axes (*X*, *Y*, *Z*, *U*, *A*, and *C*). The movement control resolution of *X* and *Y* axes is 0.1 μm, and the positioning accuracy of the *Z*–axis is below 0.05 mm. The grinding wheel is mounted on a vertical spindle, and the spindle head moves along a self–cycling linear rolling bearing guide ensuring good response characteristics. The KDP crystal is fixed onto the dynamometer by a vise, and the dynamometer is mounted on the worktable

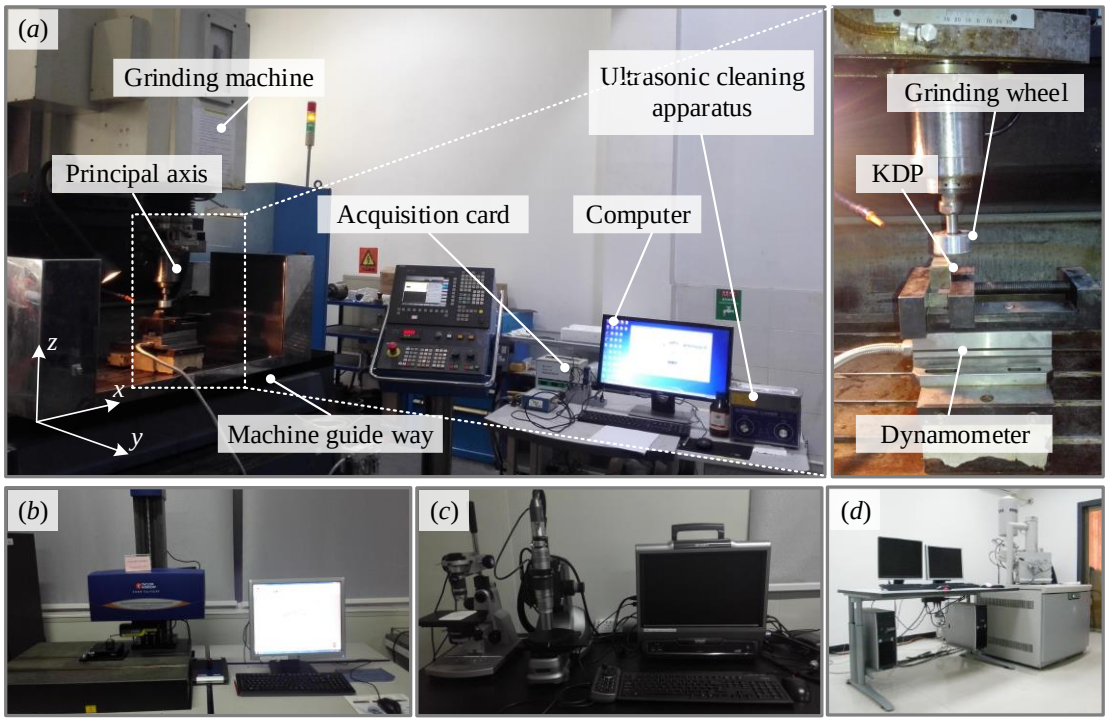

Fig. 5 Grinding test platform: (*a*) Grinding machine, (*b*) Talysurf PGI 1240, Taylor-Hobson, (*c*) VHX-1000, KEYENCE and (*d*) Scanning electron microscope

3.3 Measurements

Grinding radio *G* is evaluated. The weight change of the workpiece and grinding wheel before and after grinding is measured with a precision electronic scale. Surface roughness is measured with a contact probe profilometer (Form Talysurf PGI 1240, Taylor-Hobson; Fig. 5*b*). Ground surface morphology is measured with a 3D optical microscope (VHX-1000, KEYENCE; Fig. 5*c*). The wear types of the grinding wheels are observed under a scanning electron microscope (Fig. 5*d*). Grinding forces, which are used to calculate SGE at different material removal rate are monitored with a Kistler 9257*B* dynamometer during grinding.

3.4 Grinding procedure

Grinding tests are carried out by comparing the performance of a conventional RDGW and the newly developed BDGW. The inner and outer diameters of the abrasive layer of the RDGW are 50 mm and 36 mm, respectively. Before grinding, the RDGW is dressed with a silicon carbide dressing wheel. Fig. 6 shows the topography of the RDGW after dressing. The abrasives are randomly distributed on the wheel surface. The average abrasive size is 38 μm, and the protrusion height is approximately 10 μm.

The same level of grinding speed is achieved by applying two rotational speeds of the grinding wheel for the two wheels, which have different diameters. For example, the grinding wheel speed is 10 m/s when the rotational speeds of the grinding wheels of the BDGW and RDGW are 12000 and 3820 r/min, respectively. Table 2 shows the grinding parameters used in the tests.

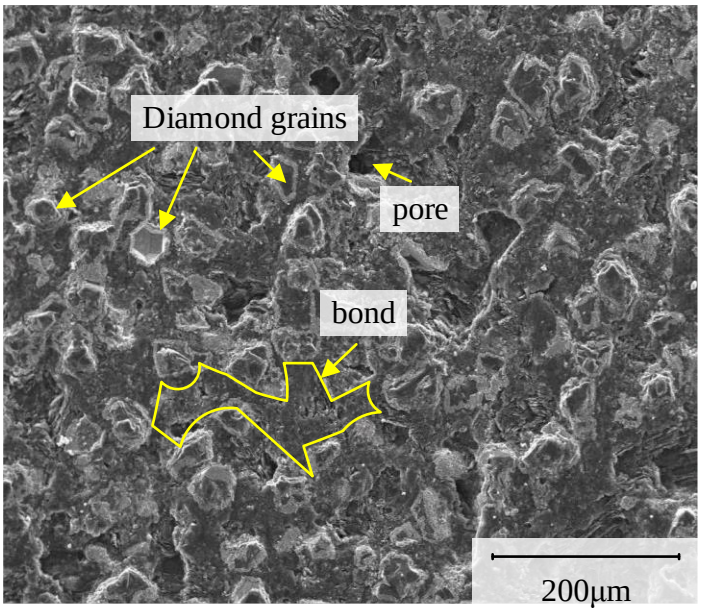

Fig. 6 Topography of RDGW

Table 2 Grinding parameters

Work-piece material	KDP crystal

Work-piece dimension	10 mm (L) × 10 mm (W) × 10 mm (H)
Worktable speed, v_w	2 mm/s,4 mm/s,6 mm/s,8 mm/s,10 mm/s
Grinding wheel speed, v_s	10 m/s
Grinding depth, a_p	10 μm
Grinding fluid	None

4. Experimental results

4.1 Grinding radio G

Grinding ratio *G* is an important index for evaluating the wear of grinding wheels. A large grinding ratio indicates small tool wear, good wear resistance and long redress life. In general, grinding radio *G* within a certain period can be calculated by using the ratio of weight change of the workpiece to that of the grinding wheel (Malkin, 1989).

$$G=\frac{W_w}{W_s} \tag{1}$$

Where: W_w is the weight change of the workpiece, and W_s is the weight change of the grinding wheel after grinding.

The grinding radio *G* of the two wheels is evaluated with the following grinding parameters: v_w = 4 mm/s, v_s = 10 m/s and a_p =10 μm. Before grinding, the weights of the workpiece and grinding wheel are measured using a precision electronic scale. After the removal of the 400 mm^3 material (400 passes), the weights of the KDP workpiece and grinding wheel are measured again. The weight changes in the workpiece and grinding wheel before and after grinding are compared, and the grinding ratio *G* is calculated. After repeating the measurements six times, the average grinding radio *G*

for the RDGW is approximately 136. In the BDGW, the weight change is almost negligible (0.001g) after 1,200 mm^3 material is removed (1,200 passes). The grinding ratio G of the BDGW is at least 10^3.

4.2 Grinding forces and specific grinding energy

The variation of grinding forces and the SGE with worktable speed are investigated at the following grinding parameters: v_s = 10 m/s, a_p =10 μm and v_w = 2-10 mm/s. In both grinding wheels, normal grinding force F_n and tangential grinding force F_t increased with worktable speed during grinding. The BDGW showed higher level of grinding forces than the RDGW, and the grinding force ratio, that is, the ratio of normal force to tangential force, showed little variations (Fig.7).

Grinding forces are strongly linked with undeformed grinding chip thickness (Agarwal and Rao, 2013). Thick grinding chips typically lead to poor surface roughness and high grinding forces. In this study, although the theoretical undeformed chip thickness are the same in both grinding wheels, the actual hardness of the BDGW is higher than that of the RDGW. Thus, the grinding depth is large, the grinding chips are thick and the grinding forces are increased. The bluntness of the abrasive edges made by laser ablation (Fig. 4) is the reason for the increases in grinding forces and SGE.

(*a*)

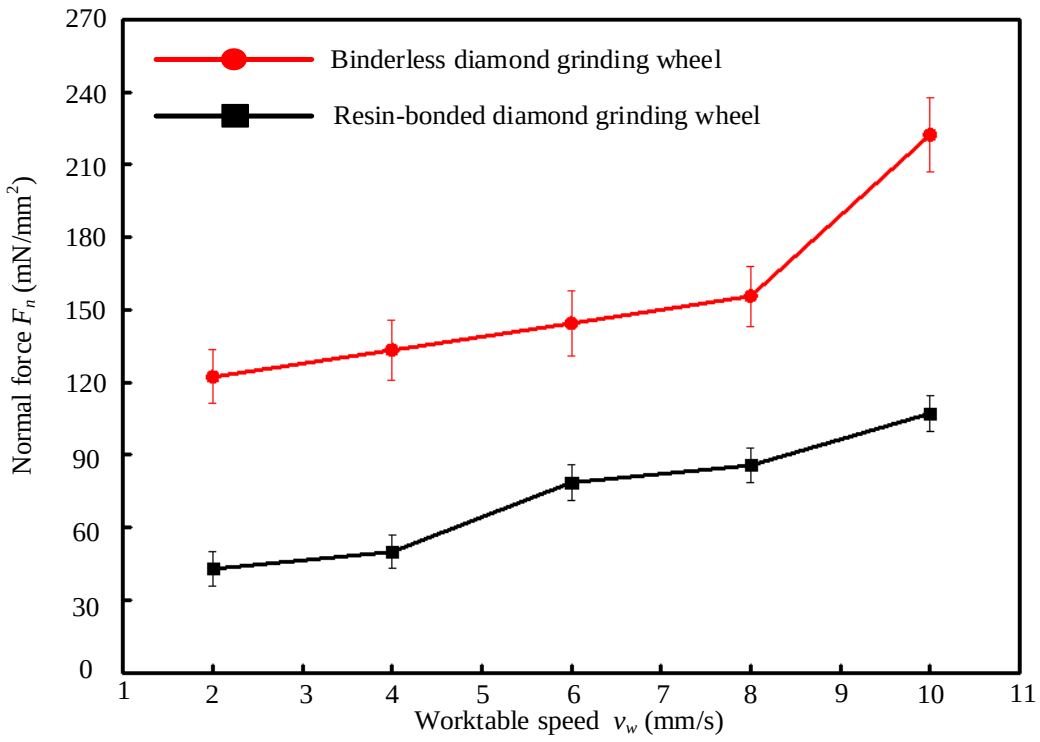
Binderless diamond grinding wheel
Resin-bonded diamond grinding wheel
Normal force F_n (mN/mm^2)
Worktable speed v_w (mm/s)
0
30
60
90
120
150
180
210
240
270
1
2
3
4
5
6
7
8
9
10
11

(*b*)

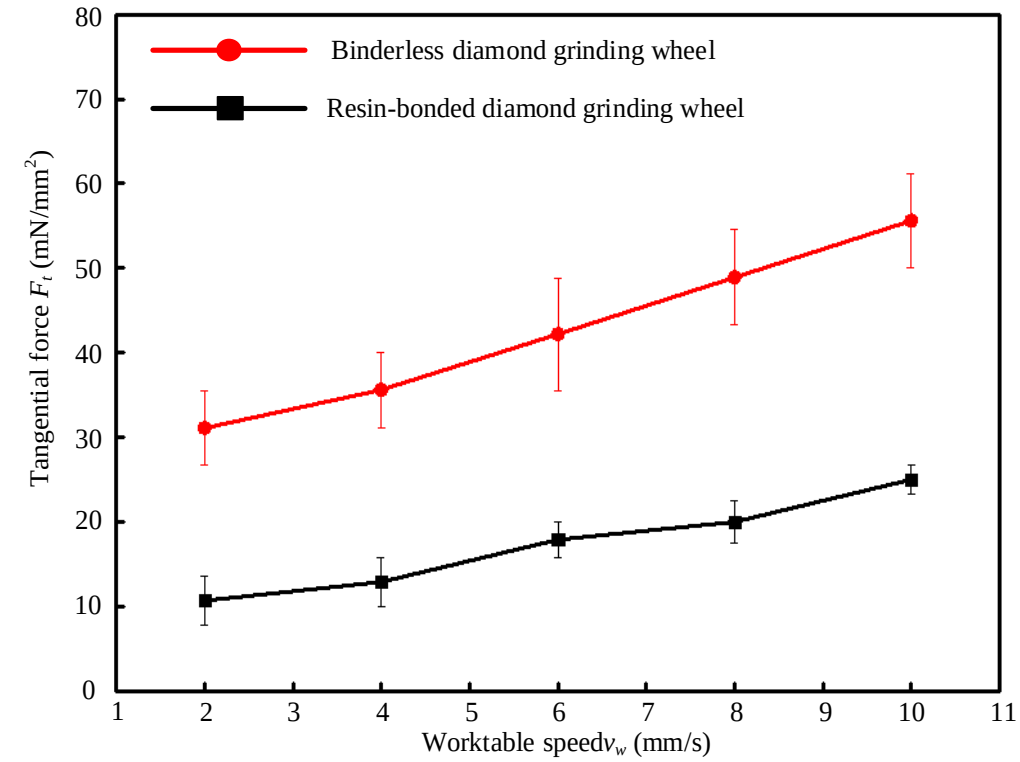
Binderless diamond grinding wheel
Resin-bonded diamond grinding wheel
Tangential force F_t (mN/mm^2)
Worktable speedv_w (mm/s)
0
10
20
30
40
50
60
70
80
1
2
3
4
5
6
7
8
9
10
11

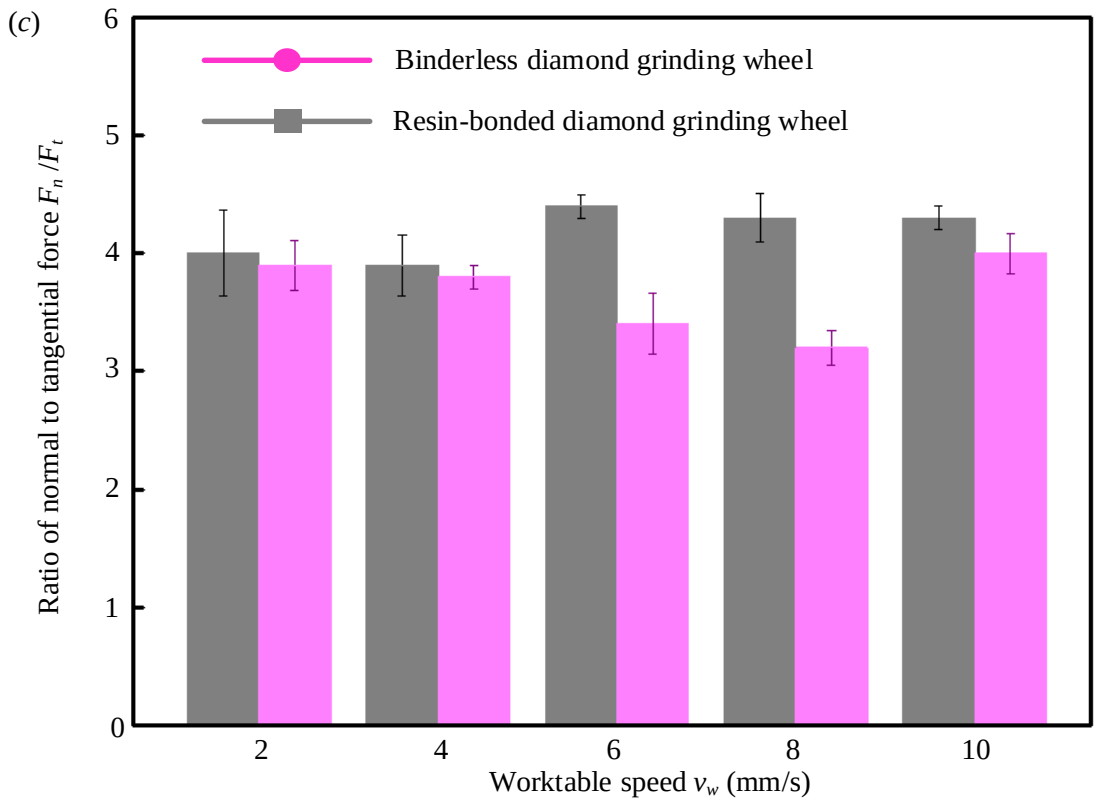

Fig. 7 Grinding forces: (*a*) normal grinding force, (*b*) tangential grinding force, and (*c*) ratio of normal to tangential grinding force

SGE (e_s) represents the energy consumed in the removal of a unit volume of a workpiece material (Malkin, 1989). The SGE of the BDGW is higher than that of the RDGW under the same grinding parameters (Fig. 8). The top of the abrasives in the BDGW has more contact areas than that in the RDGW, and thus the BDGW has higher SGE and consumes more energy to offset sliding and friction resistance in the grinding process.

$$e_s = \frac{F_t v_s}{v_w a_p b} \tag{2}$$

Where: F_t is the tangential grinding force, v_s is the speed of the grinding wheel, v_w is the worktable speed, a_p is the grinding depth and b is grinding width.

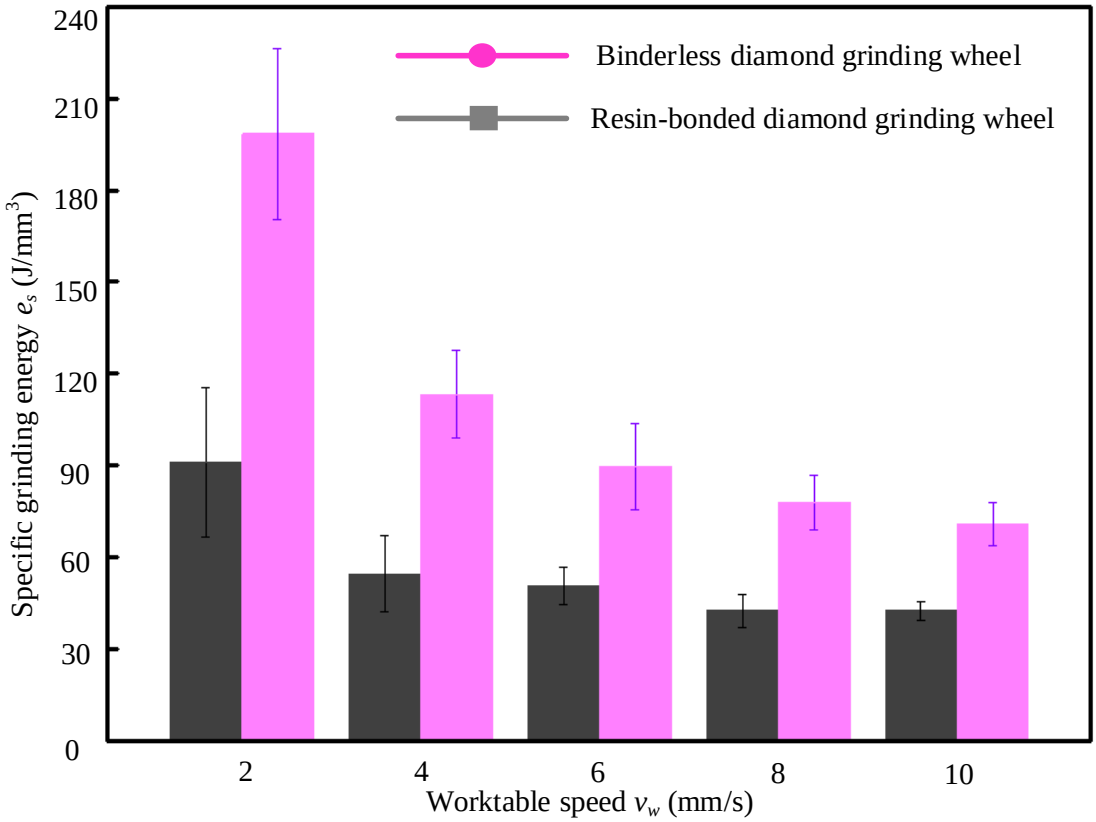

Fig. 8 Variation in specific grinding energy

4.3 Surface microtopography and surface roughness R_a

Surface microtopology and roughness R_a, which are important indices in evaluating the quality of machining surfaces, are compared at the following grinding conditions: v_s = 10 m/s, a_p = 10 μm and v_w = 2-6 mm/s. The magnification is set to 500 times for the observation of surface microtopography, and the surface roughness is measured at sampling length of 0.8 mm and evaluation length of 4 mm.

As shown in Fig. 9, the grinding marks on the ground surface are reasonably clean with plastic grinding grain and brittle flaking pits. The density of the brittle flaking pits increases with v_w. The size of the brittle flaking pits on the grinding surfaces is larger when the BDGW is used than that when the RDGW is used. Moreover, R_a increases

with v_w. When v_w = 2 mm/s, R_a after grinding with BDGW is approximately 0.48 μm, which is much higher than that after grinding with RDGW (0.24 μm).

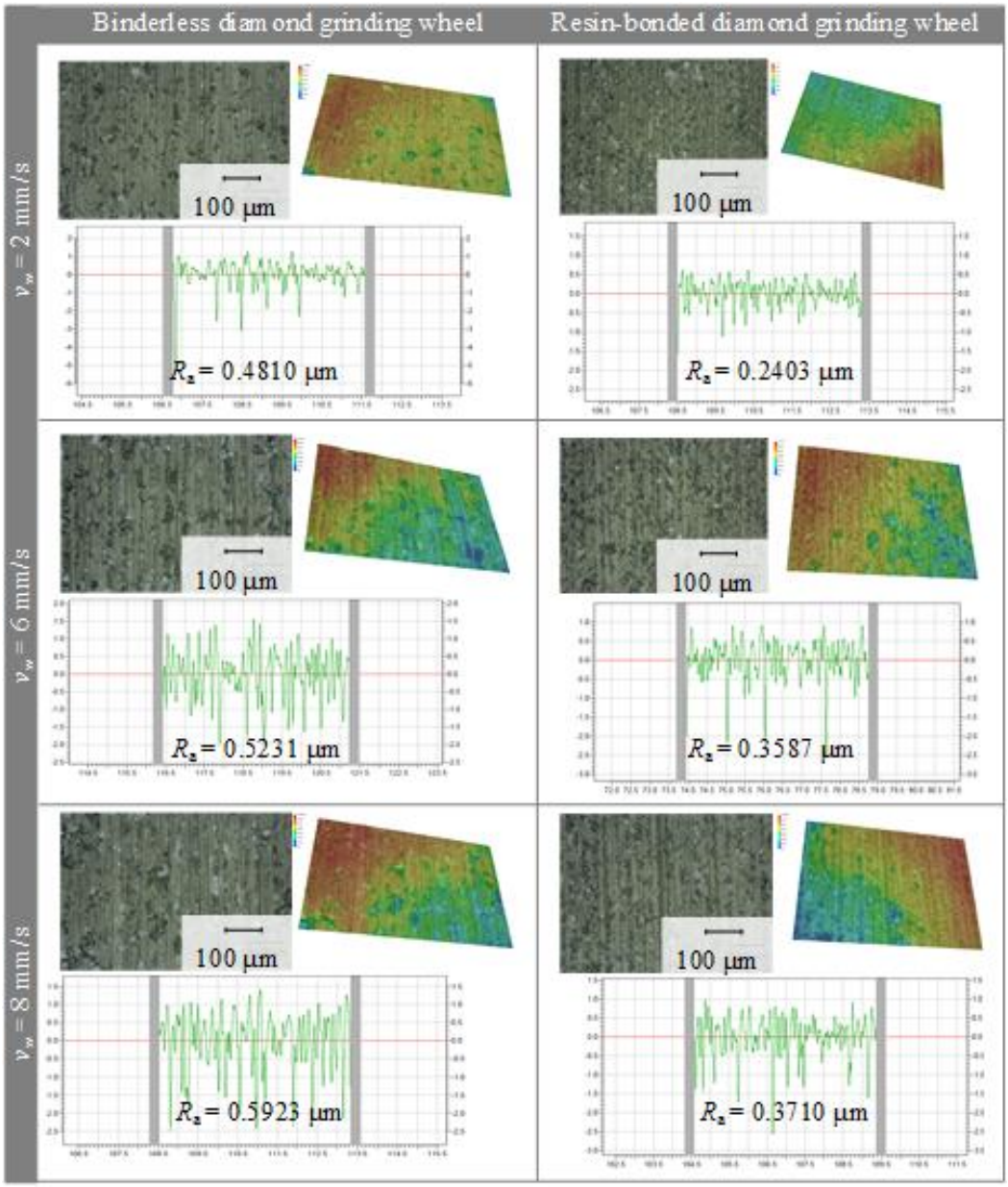

Fig. 9 Surface microstructure and roughness

4.4 Subsurface damage

Grinding induced damages can be classified into visible microcracks on the ground surface and invisible subsurface damages (SSD) caused by the penetration of median-lateral cracks at a certain depth beneath the ground surface. The depth of SSD

is a key evaluation index for assessing the surface quality of ground brittle materials. Reducing SSD decreases machining allowance for subsequent optical polishing process and thereby increases the efficiency of the overall machining process.

In this study, cross-section microscopy along the vertical direction of the ground surface is applied to determine the type, depth, and configuration of the subsurface microcracks and damages. The specific steps are as follows: (1) two processing specimens are bonded together so that the 'collapse' phenomenon caused by the edge effect of polishing is prevented; (2) the vertical direction of the machining surface is ground and polished and (3) the crack depth and microcrack configuration of the subsurface is determined by observing the surface.

SSD induced by grinding with BDGW is shown in Fig. 10. Two main forms of the SSD are observed. The maximum depth is approximately 30 μm, which is slightly deeper than the maximum depth of the conventional grinding wheel (approximately 20 μm; Qu et al., 2019). Figs. 10a and 10b show the transverse cracks, which extend to the top surface and form a fracture pit similar to a shell, with the expansion of a crack. This type crack can reduce the ground surface quality. Fig. 10c shows a radial crack, which tends to expand continuously into the crystal and increase the risk of transgranular fracture during grinding.

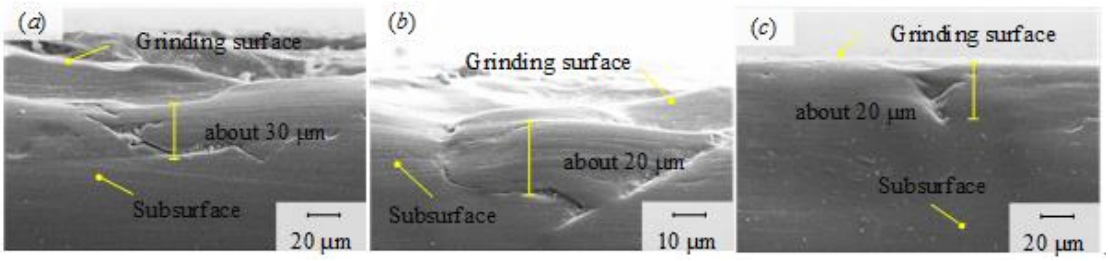

Fig. 10 Subsurface damage at v_s = 10 m/s, a_p = 10 μm and v_w = 4 mm/s: (*a*) typical of 30 μm transverse crack, (*b*) typical of 20 μm transverse crack, and (*c*) typical of 20 μm radial crack

Median crack is the main form of SSD under the action of grains. Formula 3 is the expression of the middle crack depth obtained by Randi et al. (2005) using the indentation fracture model. The median crack increases with normal load. In this study, the grains of the BDGW appears as a square cone with a flat crown on the top surface. Therefore, the grinding force on the grains is high, and the SSD increases under the same grinding parameters.

$$c_m = \alpha_\kappa^{2/3} \left(\frac{E}{H}\right)^{2(1-m_1)/3} (\cot\theta)^{4/9} \left(\frac{P}{K_{IC}}\right)^{2/3} \quad (3)$$

Where: α_κ is a dimensionless constant, $\alpha_\kappa = 0.090 \times (m_1 - 1/3) + 0.027$, m_1 ranges from 1/3 to 1/2, E is the Young's modulus of the work piece, H is the micro-hardness, K_{IC} is the fracture toughness, θ is the halt angle of a single grinding grain and P is the normal load of a single grinding grain.

5. Discussion

5.1 Grinding wheel wear

Grinding wheel wear is inevitable during grinding, because of the combined actions of mechanical, physical, and chemical syntheses. A conventional grinding wheel has many types of wear, such as abrasion, crushing, and adhesion clogging, which are due to the structures of the grinding wheels and distribution of the abrasives.

The same types of grinding wear can cause impurities embedding in the machining of soft and brittle materials with conventional grinding wheels. Scanning electron microscopy is used to observe the wear of the grinding wheels and detect surface topography after grinding. Twelve regions are evenly selected, and surface topography is used to investigate the wear of the grinding wheels. Wear in the RDGW and BDGW is shown in Figs. 11 and 12, respectively.

In this study, the conventional grinding wheel used is an RDGW, whilst the diamond abrasives are coated with Ni-P alloy. The presence of Ni-P alloy layer increases the wettability between the diamond grain and resin-bonded. As shown in Fig. 11a, a pit of approximately 20 μm is observed on the resin coating. The chippings from here may cause impurities embedding on the ground surface. In Fig. 11b, the Ni-P alloy surrounding the diamond is ground flat, indicating that the abrasive may falls off and embed in the machining surface due to weak bonding. In Fig. 11c, the majority of the coating layer of resin-bonded is removed, and a smooth wearing platform appears on the surface of the diamond grain. In Fig. 11d, the presence of gap between the bond and diamond seems to have reduced bonding ability and increase the amount of impurities embedded on the machining surface under the action of repeating grinding force.

Given the above analysis, even if the bonding ability increases because of the addition of a Ni-P alloy layer, the diamond grains still fall off and embeds in the machining surface. This condition increases not only the amount of embedded debris on the workpiece surface but also the difficulty of subsequent machining processes for the workpiece.

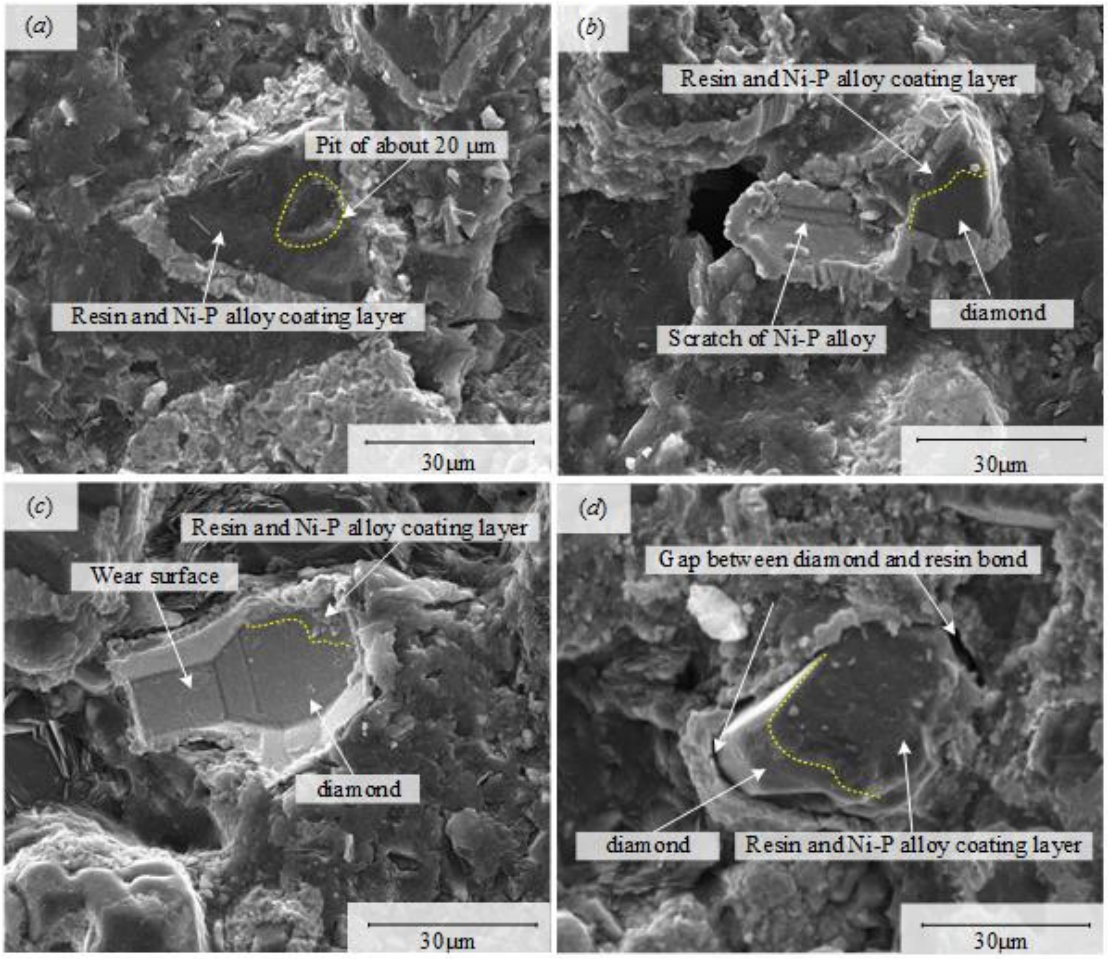

Fig. 11 Grinding wear of RDGW: (*a*) a pit of approximately 20 μm on the resin coating, (*b*) typical wear of Ni-P alloy surrounding the diamond, (*c*) typical wear of diamond grain, and (*d*) gap between the bond an diamond

Unlike in a conventional grinding wheel, the bonding features and the grains on the BGDW are produced on a single piece of CVD diamond and micro-processed with a femtosecond laser. Therefore, abrasive fall-off and bonded crack embedding can be prevented. The specific wear condition of the BDGW is shown in Fig. 12. As shown in Fig. 12a, the grains have rectangular pyramid shapes. Many tiny grains are observed on the side of the rectangular pyramid because of the coarse grain surface roughness caused by the laser ablation of the CVD diamond before grinding. After grinding, owing

to the substantial difference in hardness between the KDP crystal and the CVD diamond, the top surfaces of the grains have many small wear striations without crack tips. This phenomenon involves a typical abrasion wear with minimal impurities embedding on the machining surface. As shown in Fig. 12b, the top surfaces of the grains have small cracks. These cracks increase the risk of machining surface impurity, that is, grains are located at the middle of the grain boundary and may not sufficiently heal, resulting in the presence of residual holes or cracks. The residual holes or cracks are extended and broken, under the action of repeating grinding force.

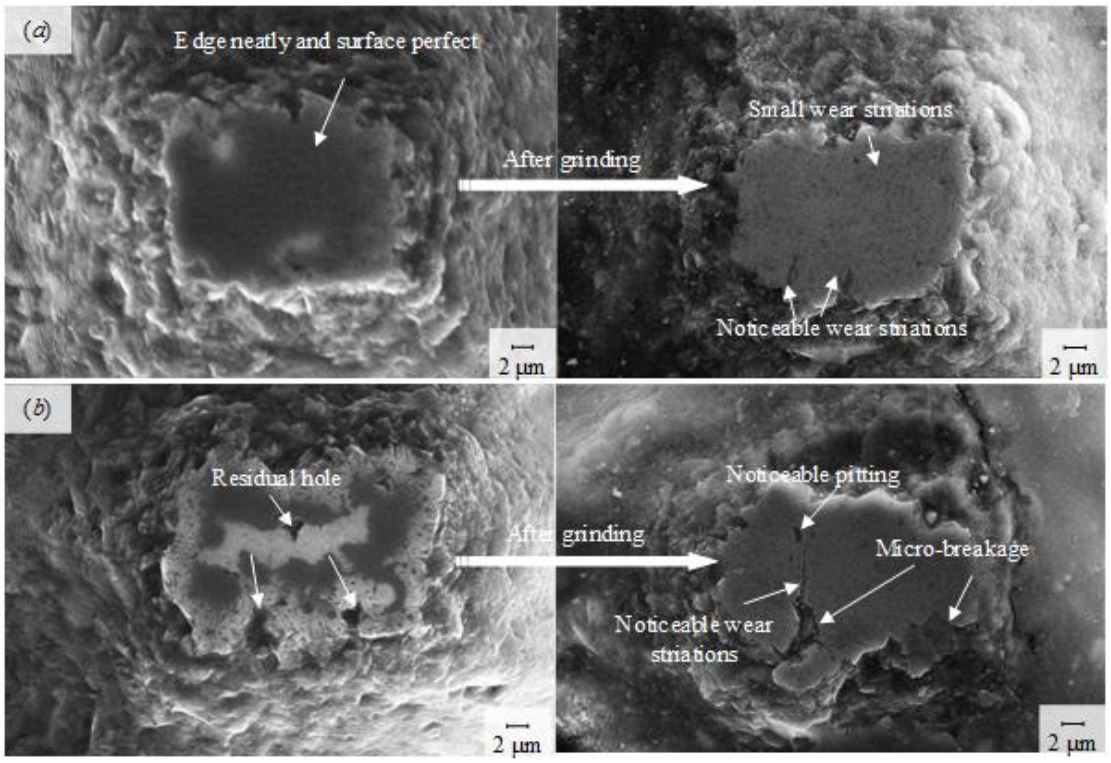

Fig. 12 Grinding wear of BDGW: (*a*) typical wear of grain with regular edge and (*b*) typical wear of grain with small cracks

6. Conclusions

A BDGW is designed and manufactured for the precision grinding of KDP crystal. The grinding performance of the newly developed wheel is investigated and evaluated by comparing the important grinding outputs of the BDGW with those of a conventional RDGW, including grinding radio, type of wheel wear, grinding forces, SGE, ground surface roughness, surface morphology, and subsurface damage.

The following conclusions are drawn from this research:

1. Large CVD diamonds can be used as abrasive layers of BDGWs. Femtosecond laser is more suitable as a micro machining method than the Q-pulse ultraviolet laser in terms of forming appropriate grains on CVD layers.

2. The grinding radio of the binderless diamond wheel can reach 10^3, which is nearly eight times that of the resin bond diamond grinding wheel (G =136).

3. Wear in the BDGW involves a simple abrasion type that prevents of embedding of bond debris or abrasive grains in KDP crystal surfaces and thus a crucial limitation when using a conventional grinding wheel, either resin-bonded or vitrified-bond, in the machining of the sensitive crystal materials.

4. Surface roughness ($R_a \leq 0.3$ μm) and subsurface damage (SSD ≤ 30 μm) are produced with the newly developed BDGW under test conditions. The ground surface quality is acceptable for the precision grinding of KDP, although slightly higher than that produced by a conventional resin-bonded diamond wheel and thus fixes the crystal axis of the KDP crystal.

5. The improvement in the surface and subsurface quality in binderless diamond grinding is still being studied, and the results will be published soon.

Acknowledgement

This work was supported by the National Science and Technology Major Project of China [No. 2014ZX04001191].

References

Agarwal, S., Rao, P. V., 2013. Predictive modeling of force and power based on a new analytical undeformed chip thickness model in ceramic grinding. J. International Journal of Machine Tools & Manufacture. 65, 68–78.

Aurich, J. C., Herzenstiel, P., Sudermann, H., Magg, T., 2008. High-performance dry grinding using a grinding wheel with a defined grain pattern. J. CIRP Annals–Manufacturing Technology. 57, 357–362.

Bespalov, V. I., Bredikhin, V. I. , Ershov, V. P., Zilberberg, V. V., 1997. Perspectives for creation of highly effective technology for fabricating KDP and KD*P crystals for ICF. J. Proceedings of SPIE. 3047, 899-902.

Brinksmeier, E., Riemer, O., Antsupov, G., Meiners, K., 2012. Manufacture and application performance of precision grinding wheels with CVD coated abrasive layers. J. International Journal of Abrasive Technology. 5, 299.

Butler-Smith, P. W., Axinte, D.A., Daine, M., 2011. Ordered diamond micro-arrays for ultra-precision grinding—An evaluation in Ti–6Al–4V. J. International Journal of Machine Tools & Manufacture. 51, 54–66.

Chen, D. S., Chen, J. H., Wang, B. R., 2016. A hybrid method for crack-less and high-efficiency ultra-precision chamfering of KDP crystal. J. International Journal of Advanced Manufacturing Technology. 87, 293–302.

Gäbler, J., Schäfer, L., Westermann, H., 2000. Chemical vapour deposition diamond coated microtools for grinding, milling and drilling. J. Diamond and Related Materials. 9, 921–924.

Gäbler, J., Pleger, S., 2010. Precision and micro CVD diamond-coated grinding tools. J. International Journal of Machine Tools & Manufacture. 50, 420–424.

Guo, B., Wu, M. T., Zhao, Q. L., Liu, H., Zhang, J., 2018. Improvement of precision grinding performance of CVD diamond wheels by micro-structured surfaces. J. Ceramics International. 44, 17333–17339.

Harniman, R. L., Fox, O. L., Janssen, W., Drijkoningen, S., Haenen, K., Paul, W. M., 2015. Direct observation of electron emission from grain boundaries in CVD diamond by PeakForce-controlled tunnelling atomic force microscopy. J. Carbon. 94, 386-395.

Heinzel, C., Rickens, K., 2009. Engineered wheels for grinding of optical glass. J. CIRP Annals–Manufacturing Technology. 58, 315–318.

Malkin, S., 1989. Grinding Technology: Theory and Application of Machining with Abrasives, New York.

Malshe, A.P., Park, B. S., Brown, W. D., Naseem, H. A., 1999. A review of techniques for polishing and planarizing chemically vapor-deposited (CVD) diamond films and substrates. J. Diamond and Related Materials. 8, 1198–1213.

Namba, Y., 1998. Ultra-precision Grinding of Optical Materials for High Power Lasers, J. Proceedings of SPIE, 3244, 320-330.

Qu, M. N., Xie, G.Z., Jin, T., Cai, R., Lu, A.G., 2019. Realization of high efficiency and low damage machining of anisotropic KDP crystal by grinding. J. Precision Engineering. 55, 464-473.

Randi, J. A., Lambropoulos, J. C., Jacobs, S. D., 2005. Subsurface damage in some single crystalline optical materials. J. Applied optics. 44, 2241-2249.

Randles, A. B. , Kuypers, J. H. , Esashi, M., Tanaka, S., 2008. Application of Lithium Niobate Etch Stop Technology to SAW Pressure Sensors. J. IEEE Ultrasonics Symposium. 1124-1127.

Tawakoli, T., Westkaemper, E., Rabiey, M., 2007. Dry grinding by special conditioning. J. Int J Adv Manuf Technol. 33, 419–424.

Walter, C., Komischke, T., Kuster, F., Wegener K., 2014. Laser-structured grinding tools – Generation of prototype patterns and performance evaluation. J. Journal of Materials Processing Technology. 214, 951–961.